Barriers for interfacial back-electron transfer: a comparison between TiO_2 and SnO_2/TiO_2 core/shell structures

Ludovic Troian-Gautier‡, Renato N. Sampaio‡, Eric J. Piechota, Matthew D. Brady, and Gerald J. Meyer*

Department of Chemistry, University of North Carolina at Chapel Hill, Chapel Hill, North Carolina, 27599, United States

‡ Both authors contributed equally

Abstract:

Temperature dependent kinetics for back-electron transfer (BET) from electrons in TiO_2 or SnO_2/TiO_2 core/shell nanoparticles to oxidized donor-bridge-acceptor (D-B-A) sensitizers is reported over a 110° range. Two D-B-A sensitizers (CF_3-**p** and CF_3-**x**) were utilized that differed only by the nature of the bridging ligand, a xylyl spacer that largely insulated the two redox active centers, and a phenyl bridge that promoted strong electronic coupling and an adiabatic electron transfer mechanism. An Arrhenius analysis revealed that the activation energies were significantly larger for the core/shell oxides, $E_a = 32 \pm 4$ kJ/mol, compared to TiO_2 alone, $E_a = 22 \pm 6$ kJ/mol. The barriers for BET on sensitized TiO_2 were within the same range as previous literature reports, while this study represents the first quantification for SnO_2/TiO_2 core/shell materials. Two different models were are proposed to rationalize the larger barrier for the core/shell materials: 1) a band edge offset model; and 2) a low energy trap state model with recombination from the TiO_2 rutile polymorph shell. The latter model was preferred and is in better agreement with the experimental data. The kinetic analysis also afforded the forward and reverse rate constants for the intramolecular equilibrium. In accordance with theoretical predictions and previous research, the absolute value of the free energy change was smaller for the adiabatic equilibrium provided by the phenyl bridge, i.e. $|\Delta G^o_{ad}| < |\Delta G^o|$.

Introduction:

Mesoporous thin films of wide bandgap metal oxide semiconductors, such as TiO_2 and SnO_2, are commonly utilized for dye-sensitized solar energy conversion and storage applications.[1-14] Dye-sensitized water oxidation with these materials requires catalysts that accept redox equivalents from the oxidized dyes and accumulate them for O_2(g) production while avoiding recombination with the injected electrons.[1, 3, 4, 10-13, 15] To this extent, the lifetime of electrons injected into TiO_2 and related metal oxide (MO_x) thin films is critically important. The microsecond lifetimes that are typical for anatase TiO_2 used in regenerative dye-sensitized solar cells are often insufficient for the much slower water oxidation reactions. In an attempt to circumvent this kinetic limitation, core/shell SnO_2/TiO_2 architectures have been utilized that inhibit interfacial charge recombination, termed hereafter "back-electron transfer" (BET), and greatly extend the lifetime of the injected electron relative to TiO_2 alone.[5-9, 16-20] As a result, the core/shell SnO_2/TiO_2 thin films exhibit higher water oxidation efficiencies when compared to their SnO_2 or TiO_2 counterparts.[11, 21-24]

Although core/shell metal oxides are commonly utilized for dye-sensitized water oxidation, the origin of the enhanced water oxidation performance and longer lifetimes of the injected electrons are still debated.[5, 16, 25] Two models have been proposed. In the first, the ~300 meV (29 kJ mol^{-1}) lower conduction band edge expected for single crystal SnO_2 relative to TiO_2 has been proposed to provide to exist within the core/shell materials thereby providing a barrier for electrons residing in the core to enter the shell.[16] In the second model, an interfacial $Sn_xTi_yO_2$ species has been proposed to be present between the core and the shell which provides a low energy trap for injected electrons.[25]

Temperature dependent back-electron transfer kinetics provide estimates of the intrinsic barrier for the rate determining BET step and hence insights into the mechanism. Standard Arrhenius analysis has previously provided activation energies (E_a) for back-electron transfer that ranged between 11 kJ mol^{-1} and 27 kJ mol^{-1} depending on the nature of the mediator or sensitizer as well as the distance between the redox center and the TiO_2 nanocrystallites.[26-29]

Herein, the underlying thermodynamic barriers for back-electron transfer for both TiO_2 and core/shell SnO_2/TiO_2 thin films are reported. The sensitizers utilized were bis(tridentate) cyclometalated Ru^{II} centers, CF_3-**x** and CF_3-**p**, covalently bound through a phenyl- or xylyl-thiophene bridge to a pendant triphenylamine (TPA) unit (**Figure 1**). Substitutions on the bridge

allowed the electronic coupling, H_{DA}, to be modulated. The phenyl bridge (R = H) facilitated strong electronic coupling and adiabatic electron transfer, $H_{DA} > 1000$ cm^{-1}, whereas the xylyl bridge (R = CH_3) resulted in smaller coupling, $H_{DA} < 150$ cm^{-1}.[30, 31] The kinetic analysis provided the equilibrium constants for the $Ru^{III/II}$-B-$TPA^{+/0}$ and the values were found to be closer to unity for the adiabatic equilibrium, *i.e.* $|\Delta G^o_{ad}| < |\Delta G^o|$.[31] The data also showed that the activation energies for back-electron transfer from electrons in SnO_2/TiO_2 core/shell to Ru^{III} or TPA^+ were consistently larger than those measured for TiO_2.

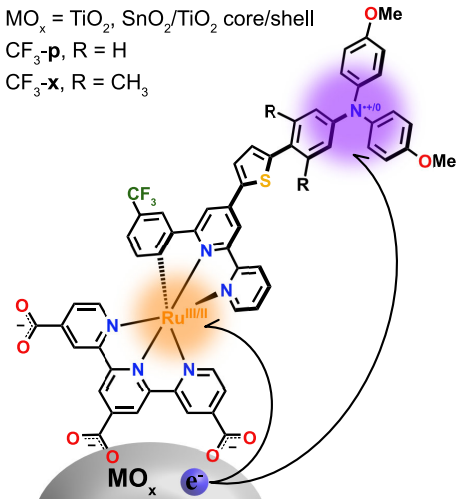

Figure 1: Structure of the D-B-A sensitizers bearing either a **x**ylyl bridge (R = CH_3, CF_3-**x**) or a **p**henyl bridge (R = H, CF_3-**p**) anchored on different metal oxides (TiO_2 or SnO_2/TiO_2 core/shell). The recombination reaction from electrons in the metal oxides to the oxidized Ru^{III} or the oxidized TPA^+ is highlighted.

Experimental:

Materials. The following reagents were used as received: titanium(IV) isopropoxide (Sigma-aldrich, 97%), polyethyleneglycol Bisphenol A Epichlorohydrin Copolymer (M. W. = 15,000-20,000 Da, Sigma-Aldrich), SnO_2 nanoparticles (15% w/v, 15 nm diameter, Alfa-Aesar), poly(ethylene oxide) (M. W. = 100,000), tetrakis(dimethyalmido) titanium (IV) (Sigma-Aldrich, 99.999%), Lithium perchlorate (Sigma Aldrich, 99.99%), Argon gas (Airgas, 99.998%), Oxygen gas (Airgas, Industrial grade), fluorine-doped tin oxide-coated glass (FTO, Hartford Glass Ci., Inc, 2.3 mm thick, 15 Ω/□). The sensitizers CF_3-**x** and CF_3-**p** were synthesized following published procedures.[32]

Preparation of SnO_2 and TiO_2 colloidal suspensions.

Colloidal TiO_2 and SnO_2 solutions were obtained following published procedures.[33-35] For SnO_2, 30 mL of SnO_2 colloid (15 wt% in H_2O) were placed in a 125 mL Erlenmeyer flask. Glacial acetic acid (1mL) was added dropwise with vigorous stirring. The mixture was stirred until the white solution became homogeneous (approximately 8h). The mixture was transferred to a 45 mL Parr reaction vessel and sealed. The reaction vessel was heated to 240°C in 1h and held at that temperature for 60h. After hydrothermal treatment, the reaction was brought to room temperature in one hour and the mixture was transferred in a vial and sonicated. PEO [poly(ethylene oxide) (M.W = 100,000)] and PEG [poly(ethylene glycol) (M.W = 15,000)] were added to reach a final concentration of 2.5 wt% of PEO and 2.5 wt% of PEG.

For TiO_2, 60 mL of deionized water were poured in a 125 mL Erlenmeyer flask. Concentrated nitric acid (70%, 0.42 mL) was then added. The solution was stirred vigorously under protection from light. Titanium (IV) isopropoxide (10 mL) was then added dropwise to that mixture. After addition, the mixture was heated at 95°C for several hours until the final volume reached 20 mL. The slurry was then transferred to a 25 mL acid digestion bomb and heated at 200°C for 12h. After digestion, the mixture was brought to room temperature and transferred into a vial. Finely ground Polyethyleneglycol Bisphenol A Epichlorohydrin Copolymer 15,000-20,000 Da (Carbowax, 1g) was then added and the mixture was stirred until complete dissolution of the carbowax occurred.

Preparation of TiO_2 and SnO_2/TiO_2 core/shell thin films.

The mesoporous TiO_2 and SnO_2 thin films were obtained following published procedures.[1, 2, 25, 34] TiO_2 or SnO_2 colloidal suspensions described above were doctor-bladed onto a fluorine-doped tin oxide (FTO) substrate to reach a thickness or approximately 3 μm and a width of 1 cm. The substrates were allowed to stand in the dark for 30 minutes prior to being heated at 450°C under a flow of O_2. The thin films were then stored in an oven kept at 70°C until needed. For core/shell SnO_2/TiO_2 thin films, the SnO_2 thin films previously prepared were modified by atomic layer deposition (ALD) of tetrakis(dimethylamido) titanium (IV) ($Ti(NMe_2)_4$, TDMAT) held at 75°C, using an Ultratech/Cambridge Nanotech Savannah S200 instrument. The chamber was kept at 130°C under 20 sccm of N_2 carrier gas flow with a deposition sequence that was as follows: 0.3 s TDMAT pulse, 30 s hold, 60 s N_2 purge, 0.02 s H_2O pulse, 30 s hold, and 60 s N_2 purge. After deposition of 75 cycles of ALD TiO_2 on SnO_2 (~ 4.5 nm, 0.06 nm/cycle), the as prepared core/shell structures were annealed at 450 °C under 1 atm O_2 for 30 min.

UV−Vis Absorption. The UV−vis absorption spectra were recorded on a Varian Cary 60 UV−Vis spectrophotometer with a resolution of 1 nm.

Transient absorption. Nanosecond transient absorption measurements were acquired on a previously described apparatus.[36] Briefly, a Q-switched, pulsed Nd:YAG laser (Quantel U.S.A. (BigSky) Brilliant B 5-6 ns full width at half-maximum (fwhm), 1 Hz, ∼10 mm in diameter) doubled to 532 nm with appropriate non-linear optics was utilized. The laser irradiance at the sample was attenuated to 0.5 mJ/pulse. The probe lamp consisted of a 150 W Xenon arc lamp that was often pulsed at 1Hz. Signal detection was achieved using a monochromator (SPEX 1702/04) optically coupled to an R928 photomultiplier tube (Hamamatsu) at a right angle to the excitation laser. Transient data were acquired with a computer-interfaced digital oscilloscope (LeCroy 9450, Dual 330 MHz) with an overall instrument response time of ∼10 ns. An average of 90 laser pulses was averaged at each wavelength of interest over the 370-800 nm range. Intervals of 10 nm were used between 390 and 800 nm.

Results:

The CF_3-**x** and CF_3-**p** sensitizers were synthesized following published procedures and were anchored on TiO_2 or SnO_2/TiO_2 core/shell (CS) thin films (abbreviated hereafter $TiO_2|CF_3$-**x/p** and CS|CF_3-**x/p**) by soaking in a concentrated methanol solution.[32] The thin films were immersed in the desired sensitizer solution until absorbance values reached 0.3-0.6 at 430 nm. Low sensitizer surface coverages were utilized to inhibit dye to oxidized dye intermolecular electron transfer (also known as lateral hole-hopping).[37-41]

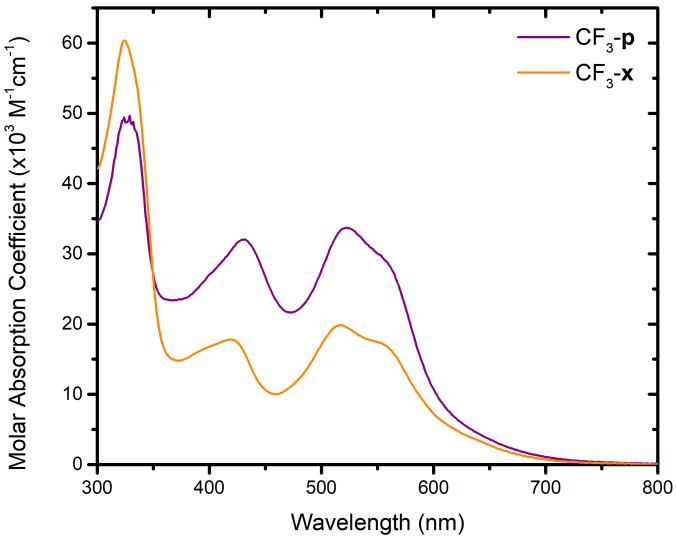

Figure 2: Absorption spectra of CF_3-**p** and CF_3-**x** recorded in methanol at room temperature.

Typical absorption spectra of CF_3-**x/p** in methanol solution are represented in **Figure 2**. The ground-state UV-vis spectra exhibited three major spectral features. First, the absorption bands at lower energy, centered around 510 nm and 600 nm, were attributed to metal-to-ligand charge transfer (MLCT) transitions. Second, the higher energy band, centered around 450 nm, was characteristic of an intra-ligand charge transfer (ILCT) transition between the cyclometalating ligand and the triphenylamine moiety. Third, the absorption features below 400 nm, which were attributed to π to π^* transitions of terpyridine, triphenylamine and the cyclometalating ligand. Detailed oxidative spectroelectrochemical studies of the sensitizers CF_3-**x** and CF_3-**p** have been previously reported in solution and anchored to metal oxide thin films.[30-32] Briefly, upon surface immobilization, CF_3-**x** and CF_3-**p** exhibited a TPA-centered oxidation with $E°(TPA^{+/0})$ = 945 mV and 955 mV vs NHE respectively, which were concomitant with the appearance of TPA^+ absorption features around 700 nm. Applying a more positive potential led to $Ru^{III/II}$ oxidation and a MLCT bleach with $E°$ ($Ru^{III/II}$) = 1010 mV and 1050 mV vs NHE for CF_3-**x** and CF_3-**p** respectively.[30]

The transient absorption difference spectra of $TiO_2|CF_3$-**x/p** and CS|CF_3-**x/p** after pulsed 532 nm light excitation in 0.1 M $LiClO_4$ CH_3CN electrolyte are represented in **Figure 3**. Pulsed light excitation led to rapid electron injection, that could not be time-resolved, from the cyclometalated Ru excited-state into the metal oxide, $MO_x|Ru^{II*} - B - TPA \rightarrow MO_x(e^-)|Ru^{III} - B - TPA$, where Ru^{II}-B-TPA denotes either CF_3-**x** or CF_3-**p** and MO_x is either TiO_2 or SnO_2/TiO_2 core/shell thin films. The nature of the bridge (B), *i.e.* thiophene-xylyl or

thiophene-phenyl, controlled the extent of electronic coupling between Ru^{III} and TPA, $MO_x(e^-)|Ru^{III}-B-TPA \rightleftharpoons MO_x(e^-)|Ru^{II}-B-TPA^+$.[31] Oxidized triphenylamine (TPA^+) exhibited very distinct absorption features above 600 nm.[42] Back-electron transfer from electrons in the metal oxide thin films to TPA^+ was monitored at 750 nm, $MO_x(e^-)|Ru^{II}-B-TPA^+ \rightarrow MO_x|Ru^{II}-B-TPA$. The corresponding back-electron transfer from CS(e^-) to TPA^+ occurred 1-2 orders of magnitude slower than for TiO_2(e^-). Indeed, the TPA^+ transient signal returned to pre-excitation levels within several hundreds of microseconds for sensitizers anchored to TiO_2 whereas it took around 0.1 seconds on SnO_2/TiO_2 core/shell nanoparticles.

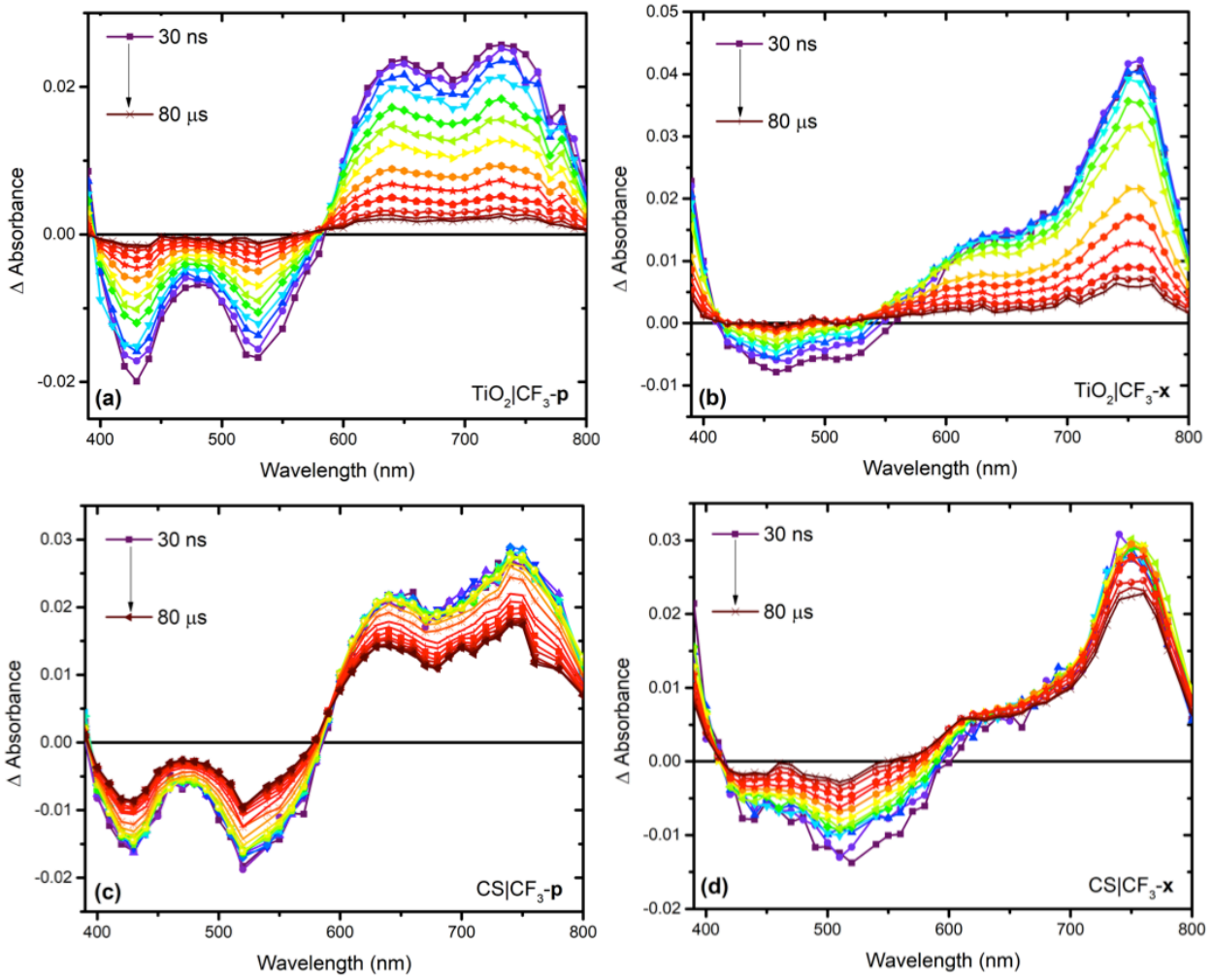

Figure 3: Transient absorption difference spectra measured over the indicated time range after pulsed 532 nm light excitation of $TiO_2|CF_3$-**p** (a), $TiO_2|CF_3$-**x** (b), $CS|CF_3$-**p** (c) and $CS|CF_3$-**x** (d) thin films submerged in argon purged 0.1M $LiClO_4$ CH_3CN electrolyte.

To gain further insight into the barriers for back-electron transfer, single wavelength absorption changes were recorded at 730 nm over a temperature range that spanned 110° (from -40°C to +70°C). Representative data for $TiO_2|CF_3$-**x/p** and $CS|CF_3$-**x/p** are represented in **Figure 4**.

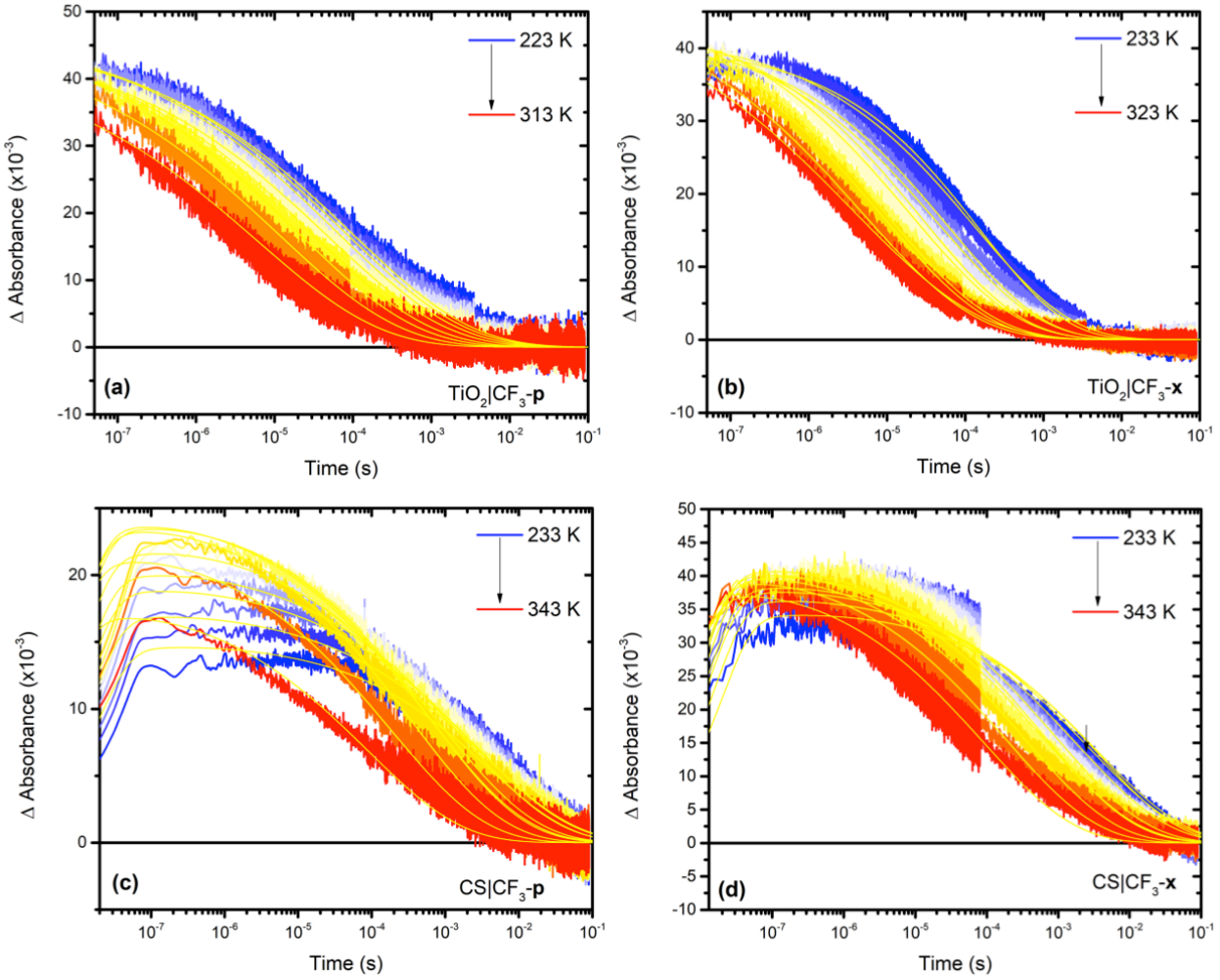

Figure 4: The absorption change monitored at 730 nm after pulsed 532 nm excitation of $TiO_2|CF_3$-**p** (a), $TiO_2|CF_3$-**x** (b)**,** $CS|CF_3$-**p** (c) and $CS|CF_3$-**x** (d) over the temperature ranges indicated. The dye-sensitized thin films were immersed in an argon purged 0.1M $LiClO_4$ CH_3CN electrolyte solution.

A previously described kinetic model[31] (*vide infra*), that accounts for both intramolecular electron transfer equilibrium between the oxidized sensitizer and the triphenylamine moiety as well as interfacial back-electron transfer to a discrete redox center, either TPA^+ or Ru^{III}, was used to quantify the experimental data. The forward and reverse rate constants for the intramolecular equilibrium extracted from this analysis were used to calculate the equilibrium constant between [Ru^{II}-B-TPA^+] and [Ru^{III}-B-TPA]. Consistent with previous studies, a van't Hoff plot of this data

(**Figure 5**) revealed an adiabatic electron transfer mechanism for CF_3-**p** on both oxides, i.e. $\Delta H^o = q_p = 0$, and a smaller equilibrium constant for the adiabatic pathway.[31] In contrast, larger equilibrium constants with a marked temperature dependence revealed a non-adiabatic pathway for CF_3-**x**, $\Delta H^o = -7$ kJ/mol.

A challenge often encountered in kinetic analysis of interfacial electron transfer lies in the non-exponential nature of the back-electron transfer reaction. There are indeed only limited examples when back-electron transfer from TiO_2 was first-order.[26, 43] A "stretched exponential" function, known as the Kohlrausch-William-Watts (KWW) function (equation 1) was used to fit the data, from which average rate constant k_{kww} was calculated (equation 2) with the Gamma function (Γ).

$$\Delta A = \sum_{i=1} \Delta A \quad e^{-(kt)^{\beta}} \qquad (1)$$

$$k_{kww} = \frac{k_i \beta}{\Gamma\left(1/\beta\right)} \qquad (2)$$

Scher and Montroll initially derived the KWW function based on a random walk model that is nowadays an archetype for modelling charge transport in disordered media.[44] In this model, β was inversely related to the width of the underlying Lévy distribution of rate constants, $0 < \beta < 1$, A_0 is the initial absorbance, k is the characteristic rate constant and k_{kww} is the average rate constant. A first-order reaction is recovered when $\beta = 1$.[26] In the present case, back-electron transfer from injected electrons to oxidized triphenylamine was fit with a β value of 0.35-0.4, and was independent of the chemical nature of the MO_x thin film.

The average rate constant, k_{kww}, extracted at each temperature for $TiO_2|CF_3$-**x/p** and CS|CF_3-**x/p** were used to determine the activation energy E_a for back-electron transfer through an Arrhenius analysis, equation 3 (**Figure 5**). Results from the Arrhenius analysis are gathered in **Table 1**.

$$\ln k = \frac{-E_a}{R}\frac{1}{T} + \ln A \quad (3)$$

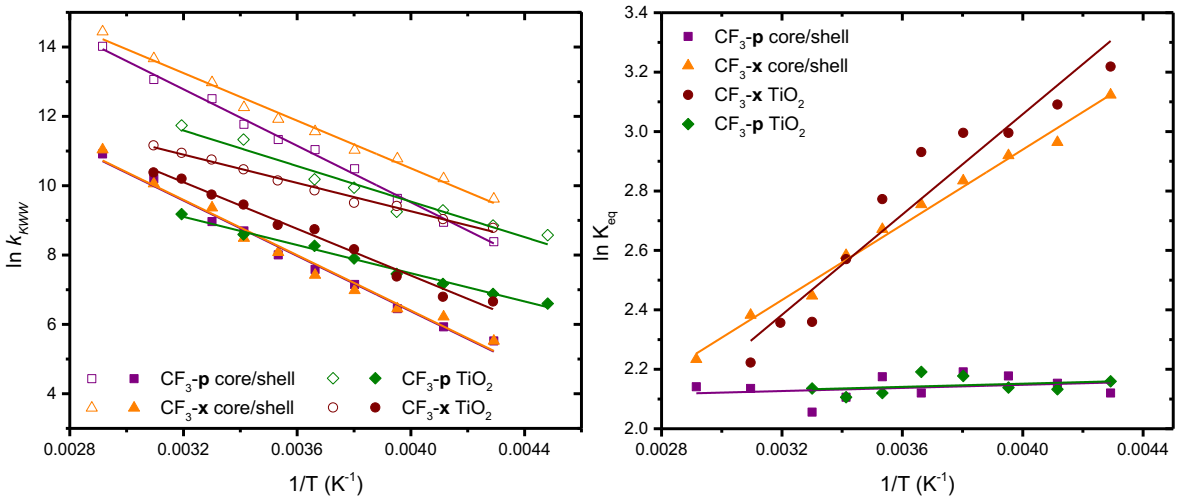

Figure 5: Arrhenius (left) analysis of back-electron transfer at the indicated dye-sensitized interfaces. The open shapes correspond to back-electron transfer from $MO_x(e^-)$ to Ru^{III} whereas the solid shapes correspond to back-electron transfer from $MO_x(e^-)$ to TPA^+. A van't Hoff plot (right) obtained from the intramolecular equilibrium between $MO_x(e^-)|Ru^{III}$-B-TPA and $MO_x(e^-)|Ru^{II}$-B-TPA^+.

Table 1: Activation parameters for the back-electron transfer reaction from TiO_2 and SnO_2/TiO_2 core/shell (CS) to the oxidized form of the indicated sensitizer.

	Ru^{III}		**TPA^+**	
	ln(A)	E_a (kJ mol^{-1})	ln(A)	E_a (kJ mol^{-1})
TiO_2|CF_3-**x**	17	17 ± 1	21	28 ± 1
TiO_2| CF_3-**p**	19	21 ± 1	18	21 ± 1
CS|CF_3-**x**	24	29 ± 1	22	33 ± 1
CS|CF_3-**p**	26	34 ± 1	23	34 ± 1

Discussion:

Two donor-bridge-acceptor sensitizers, CF_3-**p** and CF_3-**x**, were used to investigate the back-electron transfer from electrons injected into TiO_2 (or core/shell SnO_2/TiO_2) to oxidized triphenylamine moieties. Light excitation of $TiO_2|CF_3$-**x/p** and CS|CF_3-**x/p** led to electron injection into the metal oxide and formation of the oxidized sensitizer (Step 1). After excited-state electron transfer into the metal oxide thin film, intramolecular electron transfer from TPA to Ru^{III} was thermodynamically downhill.

$$\boldsymbol{MO_x}\left|Ru^{II}-B-TPA \xrightarrow{h\nu} \boldsymbol{MO_x}(\boldsymbol{e^-})\right| Ru^{III}-B-TPA \qquad \text{Step 1}$$

$$\boldsymbol{MO_x}(\boldsymbol{e^-})|Ru^{III}-B-TPA \rightleftharpoons \boldsymbol{MO_x}(\boldsymbol{e^-})|Ru^{II}-B-TPA^+ \qquad \text{Step 2}$$

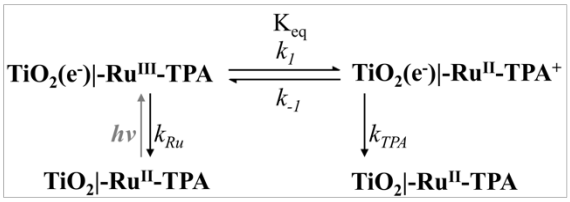

A kinetic model that incorporates both the intramolecular electron transfer equilibrium (step 2) as well as interfacial back-electron transfer to a discrete redox center was used.[31] Rate constants for back-electron transfer were measured over a 110° temperature range. Arrhenius analyses were of importance to determine the activation parameters that govern back-electron transfer from TiO_2 (or SnO_2/TiO_2 core/shell materials) to oxidized sensitizers.

Kinetic model:

The kinetic model used to extract the rate constant for back-electron transfer has been previously published and is described as follows.[31] Excited-state electron injection $MO_x|Ru^{II}$*-B-TPA $\rightarrow$ $MO_x(e^-)|Ru^{III}$-B-TPA generates the oxidized Ru sensitizer that triggers the dynamic intramolecular electron transfer equilibrium between the $Ru^{III/II}$ and $TPA^{+/0}$ redox centers, where k_1 and k_{-1} are the forward and reverse rate constants, respectively. The ground state recovery proceeds via back-electron transfer from the photo-injected electrons to either Ru^{III} (k_{Ru}) or TPA^+ (k_{TPA}). The coupled differential rate equations that mathematically describes the kinetic model are given by:

$$\frac{d[Ru^{III}]}{dt} = -(k_{Ru} + k_1)[Ru^{III}] + k_{-1}[TPA^+] \quad (6)$$

$$\frac{d[TPA^+]}{dt} = -(k_{TPA} + k_{-1})[TPA^+] + k_1[Ru^{III}] \quad (7)$$

For simplicity, $MO_x(e^-)|Ru^{III}$-B-TPA and $MO_x(e^-)|Ru^{II}$-B-TPA^+ were abbreviated to **Ru^{III}** and **TPA^+**. Equations 6 and 7 are based on first-order kinetic behavior that are appropriate for many quasi-equilibria, such as for photoacids and photobases, but may not be appropriate for charge recombination at TiO_2 interfaces when the back-electron transfer kinetics often display higher-order reaction kinetics.[45-47] The Kohlrausch-Williams-Watts (KWW) function was used to account for the non-exponential behavior,

$$f(t) = Ae^{-(k\,t)^{\beta}} \quad (8)$$

where β is inversely related to the width of an underlying Lévy distribution of rate constants. Rewriting equation 6 and 7 to consider the non-exponential nature of back-electron transfer kinetics resulted in equations 9 and 10.

$$\frac{d[Ru^{III}]}{dt} = -\left(\beta_{Ru}(k_{Ru})^{\beta_{Ru}}\, t^{\beta_{Ru}-1} + k_1\right)[Ru^{III}] + \; k_{-1}[TPA^{+}] \qquad (9)$$

$$\frac{d[TPA^{+}]}{dt} = -\left(\beta_{TPA}(k_{TPA})^{\beta_{TPA}}\, t^{\beta_{TPA}-1} + k_{-1}\right)[TPA^{+}] + \; k_1[Ru^{III}] \qquad (10)$$

The time-dependent concentrations of [Ru^{III}] and [TPA^{+}] were correlated with the absorption changes on the metal oxide thin films through a modified Beer-Lambert law, $\Delta A = \Gamma \Delta\varepsilon/1000$, where Γ is the surface coverage (mol/cm^2) and $\Delta\varepsilon$ is the extinction coefficient difference (M^{-1} cm^{-1}) between the transient state and the initial ground-state.[48]

Models for back-electron transfer

Back-electron transfer plays a paramount role in the overall efficiency of dye-sensitized solar cells (DSSCs) and dye-sensitized photoelectrosynthesis cells (DPSECs). The 1 to 2 orders of magnitude decrease in back-electron transfer timescale from electrons in core/shell SnO_2/TiO_2 compared to electrons in TiO_2 points towards drastic differences in the intrinsic electron transfer barriers for these materials. Two models proposed for back-electron transfer from core/shell are represented in **Figure 6**.

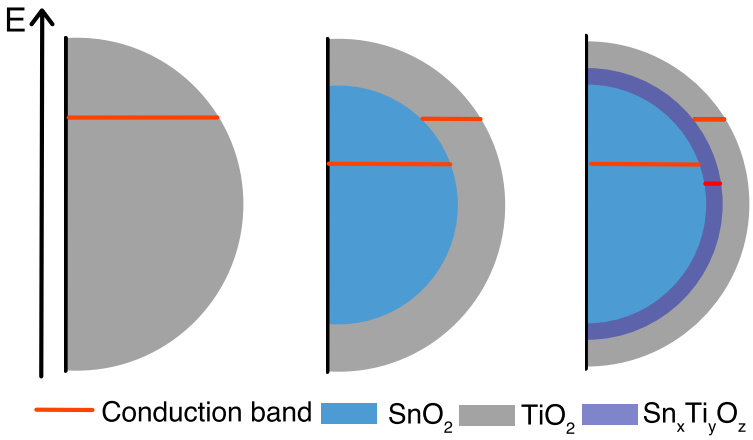

Figure 6: Representation of two models previously used to rationalize the kinetics for back-electron transfer from SnO_2/TiO_2 core/shell nanoparticles to oxidized sensitizers or redox mediators. On the left, the conduction band edge band edge potential of TiO_2 is represented for illustration purposes as a solid red line. The band edge offset model between SnO_2 and TiO_2 is represented in the middle while the formation of a low energy $Sn_xTi_yO_2$ electronic state at the interface between the SnO_2 core and the TiO_2 shell is represented on the right.

The enhanced performance of SnO_2/TiO_2 core/shell mesoporous thin films for water splitting has previously been attributed to the 300mV band edge offset between SnO_2 and TiO_2.[10, 16, 19, 22, 49] Electrons photo-injected into the TiO_2 shell migrate into the SnO_2 core and back-electron transfer is inhibited by the more negative position of the TiO_2 shell conduction band edge.[16] A second model was recently proposed based on a comparative spectroelectrochemical study of mesoporous TiO_2, SnO_2 and SnO_2/TiO_2 core/shell nanocrystallites thin films.[25] No spectroscopic evidence of electrons located either in the SnO_2 core or in the TiO_2 shell were obtained. Instead, a single reduced state was detected spectroscopically and assigned to a $Sn_xTi_yO_2$ species that formed initially in the atomic layer deposition procedure.[25] These authors also found that annealing the core/shell structures created a rutile TiO_2 shell.[25] Due to the lack of singular TiO_2 or SnO_2 absorption spectra for the reduced materials, it was suggested that the electrons were predominantly located in a discrete mixed acceptor state located at the oxide junction between the SnO_2 core and the TiO_2 shell.

The pre-exponential factor, ln(A) in the Arrhenius equation, *i.e* the frequency factor, corresponds physically to an "attempt" frequency with which the injected electrons approach the transition state imposed by the activation barrier for back-electron transfer with the oxidized sensitizer. The pre-exponential factors reported here were consistently larger for SnO_2/TiO_2 core/shell than for TiO_2. From these results, it did not seem that a slower back-electron transfer observed for SnO_2/TiO_2 core/shell originated from the "attempt" frequency. We note that the required extrapolation to infinite temperature may provide unreliable estimates of the frequency factors for BET mechanisms.

Temperature dependent back-electron transfer kinetic measurements have also proven to be useful for determination of the thermodynamic barriers for electron transfer based on spectroscopic[26-28]or photoelectrochemical assays.[50, 51] Here, activation energies for back-electron transfer of $TiO_2(e^-)$ to the TPA^+ moiety in CF_3-**x** and CF_3-**p** were measured to be 28 kJ mol^{-1} and 21 kJ mol^{-1}, respectively. These values are larger than those reported for recombination to oxidized triphenylamine mediators in solution[26, 28] as well as for electron transport between $Ti^{IV/III}$ sites in TiO_2 (0.13 eV, about 12 kJ mol^{-1}),[52] and for Li^+ transfer in $Li_{10}SnP_2S_{12}$-based composites.[53] Activation energies for electron transport in nanocrystalline TiO_2 in the range between 0.1 and 0.27 eV have also been reported.[50, 51, 54-57] The activation energies for CF_3-**x** and CF_3-**p** were however in line with those usually reported for surface anchored molecular acceptors and oxidized

sensitizers. [26-28] Indeed, back-electron transfer from $TiO_2(e^-)$ to a related "Ru-TPA" oxidized sensitizer (**Figure 7**) was determined to be 27 kJ mol^{-1}.[28] Furthermore, back-electron transfer to the oxidized ruthenium centers occured with activation energies of 17 kJ mol^{-1} and 21 kJ mol^{-1} for CF_3-**x** and CF_3-**p**, respectively. These values were within the same order of magnitude as those reported for Ru^{II} polypyridyl complexes anchored on TiO_2 interfaces.[27]

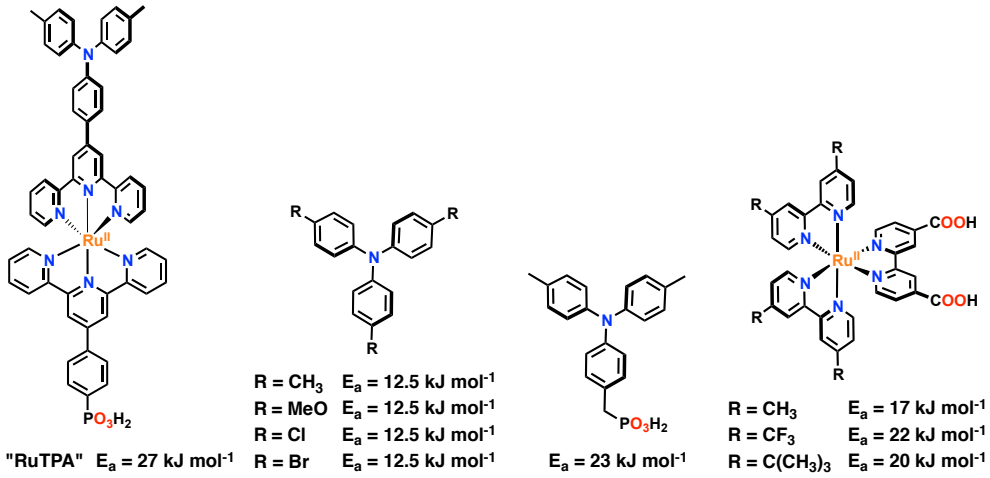

Figure 7: Activation energies for back-electron transfer from $TiO_2(e^-)$ to oxidized RuTPA,[28] triphenylamine derivatives[26, 28] and ruthenium sensitizers[27] in 0.1M $LiClO_4$ CH_3CN electrolytes.

Back-electron transfer from CS(e^-) to CF_3-**x** and CF_3-**p** occurred with activation energies that were 5 - 13 kJ mol^{-1} higher than the corresponding values obtained on TiO_2 (**Table 1**). Both models described in **Figure 6** were expected to provide significantly different activation energies than those measured for the back-electron transfer from TiO_2 and were consistent with this data. An explanation for the slower back-electron transfer from CS may arise from the different polymorphs and shell thickness that were utilized in this study. Dempsey *et al.* have concluded that electrons injected into SnO_2/TiO_2 core/shell do not reach the core when using ~ 4.5 nm shell thickness as were employed here.[16] Hence under open circuit conditions, it is possible that the injected electrons do not make it to the core or the interfacial states proposed in the two models. The TiO_2 thin films are comprised of the anatase nanocrystallites whereas a rutile TiO_2 polymorph shell is formed upon annealing of the SnO_2/TiO_2 core/shell thin films due to the rutile SnO_2 core. Swierk and Schmuttenmaer have recently shown that rutile TiO_2 was a better material for water-splitting dye-sensitized photoelectrochemical cells (WS-DSPEC) than anatase TiO_2.[58] Back-electron transfer from rutile-$TiO_2(e^-)$ to oxidized sensitizer was an order of magnitude slower than

for anatase-$TiO_2(e^-)$. Similar behavior has also been recently reported by Durrant *et al.* of anatase:rutile heterojunctions.[59] Although temperature dependent studies of back-electron transfer with the rutile polymorph of $_{TiO2}$ has not to our knowledge been conducted, the sluggish rates reported by Swierk and Durrant suggest a higher activation energy than that for anatase TiO_2, as was measured in this work.

Conclusion:

The data gathered herein provide the barriers for back-electron transfer from electrons photo-injected into metal oxide thin films to two different oxidized sensitizers. This study utilized two structurally similar Ru-B-TPA sensitizers, CF_3-**p** and CF_3-**x**, that varied only by the nature of the bridge. The phenyl-thiophene bridge allowed for strong electronic coupling between the two redox active centers while the xylyl-thiophene bridge decreased electronic coupling. A van't Hoff analysis of the equilibrium revealed an adiabatic pathway for the phenyl bridge and a non-adiabatic pathway for xylyl-bridge, where the latter preserved more Gibbs free energy. These two sensitizers were anchored onto two different MO_x thin films, TiO_2 or SnO_2/TiO_2 core/shell. Back-electron transfer from core/shell thin films was slower than from TiO_2, with higher activation energies. These observations were consistent with back-electron transfer taking place from the rutile-polymorph present in annealed SnO_2/TiO_2 core/shell thin films.

Acknowledgments

The authors acknowledge support from the Division of Chemical Sciences, Office of Basic Energy Sciences, Office of Energy Research, US Department of Energy (Grant DE-SC0013461). L. T.-G. acknowledges personal fellowships from the Belgian American Educational Foundation (BAEF) as well as the Bourse d'Excellence Wallonie-Bruxelles (WBI.World).

References

[1] L. Alibabaei *et al.*, P. Natl. Acad. Sci. USA **110** (2013) 20008.
[2] L. Alibabaei *et al.*, Nano Lett. **14** (2014) 3255.
[3] M. K. Brennaman *et al.*, J. Am. Chem. Soc. **138** (2016) 13085.
[4] J. J. Concepcion *et al.*, P. Natl. Acad. Sci. USA **109** (2012) 15560.
[5] M. K. Gish *et al.*, J. Phys. Chem. Lett. **7** (2016) 5297.
[6] M. Kapilashrami *et al.*, Chem. Rev. **114** (2014) 9662.
[7] M. Karlsson *et al.*, CHIMIA International Journal for Chemistry **67** (2013) 142.
[8] E. Palomares *et al.*, Chem. Commun. (2002) 1464.

[9] E. Palomares *et al.*, J. Am. Chem. Soc. **125** (2003) 475.
[10] B. D. Sherman *et al.*, J. Phys. Chem. Lett. **6** (2015) 3213.
[11] J. R. Swierk, and T. E. Mallouk, Chem. Soc. Rev. **42** (2013) 2357.
[12] P. Xu *et al.*, P. Natl. Acad. Sci. USA (2018)
[13] Y. Zhao *et al.*, P. Natl. Acad. Sci. USA **109** (2012) 15612.
[14] M. Grätzel, Nature **414** (2001) 338.
[15] K. Hu *et al.*, Inorg. Chem. **57** (2018) 486.
[16] R. R. Knauf *et al.*, J. Phys. Chem. C **119** (2015) 28353.
[17] M. D. Brady *et al.*, J. Am. Chem. Soc. **139** (2017) 15612.
[18] M. D. Brady *et al.*, ACS Appl. Mater. Interfaces **10** (2018) 31312.
[19] S. Chappel, S.-G. Chen, and A. Zaban, Langmuir **18** (2002) 3336.
[20] W. Li *et al.*, Chem. Soc. Rev. (2018) DOI: 10.1039/C8CS00443A
[21] L. Alibabaei *et al.*, P. Natl. Acad. Sci. USA **112** (2015) 5899.
[22] M. V. Sheridan *et al.*, ACS Energy Lett. **1** (2016) 231.
[23] D. Wang *et al.*, J. Am. Chem. Soc. **139** (2017) 14518.
[24] P. Xu, N. S. McCool, and T. E. Mallouk, Nano Today **14** (2017) 42.
[25] E. M. James, T. J. Barr, and G. J. Meyer, ACS Applied Energy Materials **1** (2018) 859.
[26] B. N. DiMarco *et al.*, Chem. Sci. **9** (2018) 940.
[27] R. N. Sampaio, B. N. DiMarco, and G. J. Meyer, ACS Energy Lett. **2** (2017) 2402.
[28] L. Troian-Gautier *et al.*, J. Am. Chem. Soc. **140** (2018) 3019.
[29] D. Kuciauskas *et al.*, J. Phys. Chem. B **105** (2001) 392.
[30] E. J. Piechota *et al.*, J. Am. Chem. Soc. **140** (2018) 7176.
[31] R. N. Sampaio *et al.*, P. Natl. Acad. Sci. USA **115** (2018) 7248.
[32] K. Hu *et al.*, Nature Chem. **8** (2016) 853.
[33] S. Chappel, and A. Zaban, Sol. Energ. Mat. Sol. C. **71** (2002) 141.
[34] T. A. Heimer *et al.*, Inorg. Chem. **35** (1996) 5319.
[35] B. O'Regan *et al.*, J. Phys. Chem **94** (1990) 8720.
[36] R. Argazzi *et al.*, Inorg. Chem. **33** (1994) 5741.
[37] B. N. DiMarco *et al.*, J. Phys. Chem. C **120** (2016) 14226.
[38] D. Moia *et al.*, J. Am. Chem. Soc. **138** (2016) 13197.
[39] T. C. Motley, and G. J. Meyer, J. Phys. Chem. C **122** (2018) 14420.
[40] J. Nelson, and R. E. Chandler, Coord. Chem. Rev. **248** (2004) 1181.
[41] K. Hu, and G. J. Meyer, Langmuir **31** (2015) 11164.
[42] K. Sreenath *et al.*, J. Phys. Chem. A **113** (2009) 6477.
[43] T. J. Barr, and G. J. Meyer, ACS Energy Lett. **2** (2017) 2335.
[44] H. Scher, and E. W. Montroll, Phys. Rev. B **12** (1975) 2455.
[45] C. A. Kelly *et al.*, Langmuir **15** (1999) 731.
[46] J. N. Demas, in *Excited State Lifetime Measurements*, edited by J. N. Demas (Academic Press, 1983), pp. 43.
[47] R. M. O'Donnell *et al.*, J. Am. Chem. Soc. **138** (2016) 3891.
[48] S. A. Trammell, and T. J. Meyer, J. Phys. Chem. B **103** (1998) 104.
[49] L. Kavan *et al.*, J. Am. Chem. Soc. **118** (1996) 6716.
[50] B. C. O'Regan, and J. R. Durrant, J. Phys. Chem. B **110** (2006) 8544.
[51] T. J. Savenije *et al.*, Chem. Phys. Lett. **461** (2008) 93.
[52] G. Boschloo, and A. Hagfeldt, J. Phys. Chem. B **109** (2005) 12093.
[53] M. Kaus *et al.*, J. Phys. Chem. C **121** (2017) 23370.
[54] A. Goossens, B. van der Zanden, and J. Schoonman, Chem. Phys. Lett. **331** (2000) 1.
[55] H. Greijer Agrell, G. Boschloo, and A. Hagfeldt, J. Phys. Chem. B **108** (2004) 12388.

[56] N. Kopidakis *et al.*, Phys. Rev. B **73** (2006) 045326.
[57] L. M. Peter *et al.*, J. Phys. Chem. B **110** (2006) 13694.
[58] J. R. Swierk *et al.*, ACS Energy Lett. **1** (2016) 603.
[59] A. Kafizas *et al.*, J. Phys. Chem. A **120** (2016) 715.